

Regular and chaotic states in a local map description of sheared nematic liquid crystals

S. M. Kamil,^{*} Sudeshna Sinha,[†] and Gautam I. Menon[‡]

The Institute of Mathematical Sciences, C.I.T. Campus, Taramani, Chennai 600013, India

(Received 25 January 2008; revised manuscript received 10 April 2008; published 18 July 2008)

We propose and study a local map capable of describing the full variety of dynamical states, ranging from regular to chaotic, obtained when a nematic liquid crystal is subjected to a steady shear flow. The map is formulated in terms of a quaternion parametrization of rotations of the local frame described by the axes of the nematic director, subdirector, and the joint normal to these, with two additional scalars describing the strength of ordering. Our model yields kayaking, wagging, tumbling, aligned, and coexistence states, accommodated in a phase diagram which closely resembles phase diagrams obtained using representations of the dynamics which are based on ordinary differential equations. We also study the behavior of the map under periodic perturbations of the shear rate. Such a map can serve as a building block for the construction of lattice models of the complex spatiotemporal states predicted for sheared nematics.

DOI: [10.1103/PhysRevE.78.011706](https://doi.org/10.1103/PhysRevE.78.011706)

PACS number(s): 61.30.Cz, 05.45.-a, 52.25.Gj, 66.20.Cy

Driven complex fluids exhibit an unusual variety of dynamical states [1–7]. When such fluids are sheared uniformly, the stress response is regular at very small shear rates. However, at larger shear rates the response is often intrinsically unsteady, exhibiting oscillations in space and time as a prelude to intermittency and chaos [6–8].

Such chaos associated with rheological response or “rheochaos” occurs in regimes where the Reynolds number is very small. It must thus be a consequence of constitutive and not convective nonlinearities, originating in the coupling of the flow to structural or orientational variables describing the local state of the fluid [9,10]. The diverse possibilities for internal degrees of freedom in complex fluids, such as the orientation of nematogenic molecules, layer stacking in lamellar and onion phases, and heterogeneities arising from local jamming in colloidal suspensions, implies that the study of the rheology of complex fluids should illuminate a variety of nontrivial steady states in driven soft matter.

Recent rheological studies of “living polymers,” solutions of wormlike micelles in which the energies for scission and recombination are thermally accessible, obtain an oscillatory response to steady shear at low shear rates which turns chaotic at larger shear rates [6,7]. It has been argued that a hydrodynamic description of this behavior requires a field describing the local orientation of the polymer, motivating a treatment of the problem of an orientable fluid, such as a nematic, in a uniform shear flow [11–13].

Nonlinear relaxation equations for the symmetric, traceless second rank tensor \mathbf{Q} characterizing local order in a sheared nematic have been derived [11–18]. Assuming spatial uniformity, a system of five coupled ordinary differential equations (ODEs) for the five independent components of \mathbf{Q} in a suitable tensor basis is obtained. Solving this system of equations yields a complex phase diagram admitting many states—aligned, tumbling, wagging, kayak-wagging, kayak-tumbling, and chaotic—as functions of the shear rate $\dot{\gamma}$ and a

phenomenological relaxation time which is a parameter in the equations of motion [19–21]. Recent work adds spatial variations: Numerical studies of the partial differential equations thus obtained yield a phase diagram containing spatiotemporally regular, intermittent, and chaotic states [22,23].

The degrees of freedom which enter a coarse-grained description of an orientable fluid are mesoscopic. Spatiotemporal structure arises from the coupling of locally ordered regions, through processes such as molecular diffusion, flow-induced dissipation, and advection. A powerful approach to understanding complex spatiotemporal dynamics is based on the study of coupled map lattices, a numerical scheme in which maps placed on the sites of a lattice evolve both via local dynamics as well as through couplings to neighboring sites [24]. However, the utility of this methodology in a specific context is often severely limited by the availability of local maps able to describe the spatially uniform case. This paper addresses this requirement in the context of a model for rheochaos, proposing the first local map description of the regular and chaotic states obtained in sheared nematics.

There is, in general, no systematic procedure for the construction of such maps. However, it is reasonable to require that any such map should accurately reproduce the full variety of states obtained through the study of the corresponding ODEs. It should also enable useful physical insights through a sensible choice of physical variables. One obvious possibility is simply the discretization of the governing ODEs. Such a choice of variables, however, is not particularly illuminating as these equations are formulated in terms of the components of \mathbf{Q} in a specific space-fixed tensor basis, rather than in terms of variables more natural to the problem.

We have thus explored an alternative formulation of this problem, constructing a local map in terms of quaternion variables. These variables encode the dynamics of the orthogonal set of axes associated with the eigenvectors of \mathbf{Q} , i.e., the director, subdirector, and the joint normal to these. Our approach incorporates biaxiality, is formulated in terms of physically accessible variables, and is computationally straightforward to implement. Our results, summarized in the phase diagram of Fig. 1, are in good agreement with previous work based on ODEs [21,28], but provide an efficient alternative to such methods [25].

^{*}kamil@imsc.res.in

[†]sudeshna@imsc.res.in

[‡]menon@imsc.res.in

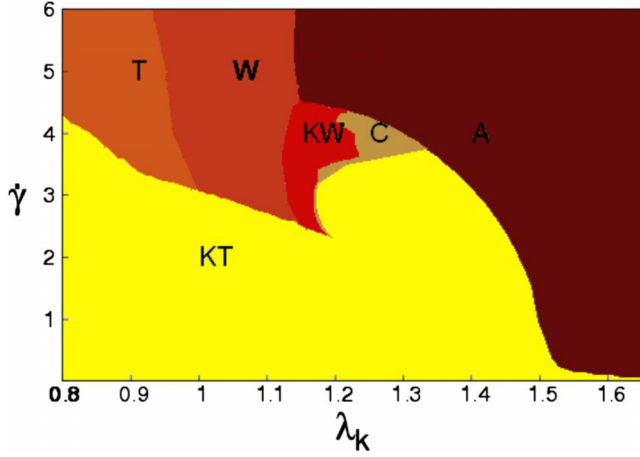


FIG. 1. (Color online) The phase diagram of steady states in our model, plotted as a function of λ_k and the shear rate $\dot{\gamma}$ (see text for definitions), illustrating regimes in which the following steady states are obtained for a generic initial condition: An aligned state denoted as A, a tumbling state labeled as T, a wagging state W, a kayak-tumbling state KT, a kayak-wagging state denoted by KW, and a complex state denoted as C. This phase diagram closely resembles phase diagrams plotted in Ref. [21].

Defining $\hat{\mathbf{b}} = \frac{1}{2}(\mathbf{b} + \mathbf{b}^T) - \frac{1}{3}(\text{tr } \mathbf{b})\delta$ to be the symmetric-traceless part of the second-rank tensor \mathbf{b} , the equation of motion for \mathbf{Q} in a passive velocity field is [11,21]

$$\frac{d\mathbf{Q}}{dt} - 2\widehat{\boldsymbol{\Omega}} \cdot \mathbf{Q} - 2\sigma\widehat{\boldsymbol{\Gamma}} \cdot \mathbf{Q} + \tau_Q^{-1}\boldsymbol{\Phi} = -\sqrt{2}\frac{\tau_{ap}}{\tau_a}\boldsymbol{\Gamma}, \quad (1)$$

where the tensor $\boldsymbol{\Omega} = \frac{1}{2}[(\nabla\mathbf{v})^T - \nabla\mathbf{v}]$, $\boldsymbol{\Gamma} = \frac{1}{2}[(\nabla\mathbf{v})^T + \nabla\mathbf{v}]$, and $\nabla\mathbf{v}$ is the velocity gradient tensor, with $\mathbf{v} = \dot{\gamma}y\mathbf{e}_x$, where \mathbf{e}_x is a unit vector in the x direction. The velocity is along the x direction the velocity gradient is along the y direction, while z is the vorticity direction. The quantities $\tau_a > 0$ and τ_{ap} are phenomenological quantities related to relaxation times, σ describes the change of alignment caused by $\boldsymbol{\Gamma}$ and $\boldsymbol{\Phi} = \partial\phi/\partial\mathbf{Q}$, with $\phi(\mathbf{Q}) = \frac{1}{2}\mathbf{A}\mathbf{Q}:\mathbf{Q} - \frac{1}{3}\sqrt{6}B(\mathbf{Q}:\mathbf{Q})^2 + \frac{1}{4}C(\mathbf{Q}:\mathbf{Q})^3$. The notation $\mathbf{Q}:\mathbf{Q}$ represents $Q_{ij}Q_{ji}$, with repeated indices summed over. Here $A = A_0(1 - T^*/T)$, and B and C are constrained by the conditions $A_0 > 0$, $B > 0$, $C > 0$, and $B^2 > \frac{9}{2}A_0C$.

Scaling $t = t^*\tau_a/A_k$, $\mathbf{v} = \mathbf{v}^*A_k/\tau_a$, and $a = a^*a_k$, Eq. (1) can be written in dimensionless form, $\frac{d\mathbf{Q}^*}{dt^*} - 2\widehat{\boldsymbol{\Omega}}^* \cdot \mathbf{Q}^* - 2\sigma\widehat{\boldsymbol{\Gamma}}^* \cdot \mathbf{Q}^* + (\theta\mathbf{Q}^* - 3\sqrt{6}\widehat{\mathbf{Q}}^* \cdot \mathbf{Q}^* + 2(\mathbf{Q}^*:\mathbf{Q}^*)\mathbf{Q}^*) = \sqrt{\frac{3}{2}}\lambda_k\boldsymbol{\Gamma}^*$, where $A_k = A_0(1 - T^*/T_k) = 2B^2/9C$, $a_k = a_{eq}(T_k) = 2B/3C$ is the (non-zero) equilibrium value of the scalar order parameter a at the transition temperature T_k , $\lambda_k = -\frac{2}{3}\sqrt{3}\frac{\tau_{ap}}{\tau_a a_k}$ and $\theta = (1 - \frac{T^*}{T})/(1 - \frac{T^*}{T_k})$ is the reduced temperature.

The \mathbf{Q} tensor admits the following parametrization: $Q_{ij} = \frac{3s_1}{2}(n_i n_j - \frac{1}{3}\delta_{ij}) + \frac{s_2}{2}(m_i m_j - l_i l_j)$, where s_1 and s_2 represent the magnitude of the ordering along \mathbf{n} (the director) and \mathbf{m} (the subdirector), with \mathbf{n} and \mathbf{m} unit vectors and $\mathbf{l} = \mathbf{n} \times \mathbf{m}$. The dynamics of \mathbf{Q} thus involves both the dynamics of the frame defined by \mathbf{n} , \mathbf{m} , and \mathbf{l} as well as the dynamics of s_1 and s_2 .

The frame dynamics can be represented in many equivalent ways, such as through coordinate matrices, axis-angle or Euler-angle representations. However, the coordinate matrix representation requires a large number of parameters, the axis-angle representation suffers from redundancy, and the use of the Euler-angle representation is marred by the ‘‘gimbal-lock’’ problem [26]. Our parametrization of the frame dynamics uses quaternion variables, providing an elegant, compact, and numerically stable alternative to these representations.

Equations for $\dot{\mathbf{n}}$, $\dot{\mathbf{m}}$, and $\dot{\mathbf{l}}$ as well as for the order parameter amplitudes \dot{s}_1 and \dot{s}_2 can be derived by considering a reference frame in which the director and subdirector are stationary (body frame). In the body frame, denoted by primed vectors, the director can be chosen to be $\mathbf{n}' = (1, 0, 0)$, and the subdirector to be $\mathbf{m}' = (0, 1, 0)$, with $\mathbf{l}' = (0, 0, 1)$. The transformation matrix \mathbf{A} which maps vectors from the laboratory frame to the body frame, can be defined in terms of quaternion parameters (e_0, \dots, e_3) constrained by $e_0^2 + e_1^2 + e_2^2 + e_3^2 = 1$. This transformation matrix has the form

$$\mathbf{A} = \begin{pmatrix} n_x & n_y & n_z \\ m_x & m_y & m_z \\ l_x & l_y & l_z \end{pmatrix} = \begin{bmatrix} e_0^2 + e_1^2 - e_2^2 - e_3^2 & 2(e_1 e_2 + e_0 e_3) & 2(e_1 e_3 - e_0 e_2) \\ 2(e_1 e_2 - e_0 e_3) & e_0^2 - e_1^2 + e_2^2 - e_3^2 & 2(e_2 e_3 - e_0 e_1) \\ 2(e_1 e_3 + e_0 e_2) & 2(e_2 e_3 - e_0 e_1) & e_0^2 - e_1^2 - e_2^2 + e_3^2 \end{bmatrix}.$$

The quantities $\mathbf{n} = (n_x, n_y, n_z)$, $\mathbf{m} = (m_x, m_y, m_z)$, and $\mathbf{l} = (l_x, l_y, l_z)$ are easily obtained using this mapping, yielding ODEs for the parameters $s_1, s_2, e_0, e_1, e_2, e_3$. These are converted into a map using a first-order Euler scheme. After each discrete time step, we renormalize the quaternion variable. Choosing σ and θ equal to zero for all of the results reported here in common with earlier work, our map is then defined through

$$s_1^{t+1} = s_1^t + \Delta \left(\frac{1}{6}(9\sqrt{6}s_1^2 - 18s_1^3 - 3\sqrt{6}s_2^2 - 6s_1s_2^2 + 3\sqrt{6}n_x n_y \dot{\gamma} \lambda_k) \right)^t,$$

$$s_2^{t+1} = s_2^t + \Delta \left(-3\sqrt{6}s_1 s_2 - 3s_2^2 s_2 - s_2^3 - \sqrt{\frac{3}{2}}(l_x l_y - m_x m_y) \dot{\gamma} \lambda_k \right)^t,$$

$$e_0^{t+1} = e_0^t + \Delta \left[\frac{1}{4}\dot{\gamma}e_3 + \frac{1}{4}\sqrt{\frac{3}{2}}\dot{\gamma} \left(-\frac{(l_y m_x + l_x m_y)e_1}{s_2} + \frac{2(l_y n_x + l_x n_y)e_2}{3s_1 + s_2} + \frac{2(m_y n_x + m_x n_y)e_3}{-3s_1 + s_2} \right) \lambda_k \right]^t,$$

$$\begin{aligned}
 e_1^{t+1} &= e_1^t + \Delta \left[\frac{1}{4} \dot{\gamma} e_2 + \frac{1}{4} \sqrt{\frac{3}{2}} \dot{\gamma} \left(\frac{(l_y m_x + l_x m_y) e_0}{s_2} \right. \right. \\
 &\quad \left. \left. - \frac{2(m_y n_x + m_x n_y) e_2}{-3s_1 + s_2} + \frac{2(l_y n_x + l_x n_y) e_3}{3s_1 + s_2} \right) \lambda_k \right]^t, \\
 e_2^{t+1} &= e_2^t + \Delta \left[-\frac{1}{4} \dot{\gamma} e_1 + \frac{1}{4} \sqrt{\frac{3}{2}} \dot{\gamma} \left(-\frac{2(l_y n_x + l_x n_y) e_0}{3s_1 + s_2} \right. \right. \\
 &\quad \left. \left. + \frac{2(m_y n_x + m_x n_y) e_1}{-3s_1 + s_2} + \frac{(l_y m_x + l_x m_y) e_3}{s_2} \right) \lambda_k \right]^t, \\
 e_3^{t+1} &= e_3^t + \Delta \left[-\frac{1}{4} \dot{\gamma} e_0 + \frac{1}{4} \sqrt{\frac{3}{2}} \dot{\gamma} \left(-\frac{2(m_y n_x + m_x n_y) e_0}{-3s_1 + s_2} \right. \right. \\
 &\quad \left. \left. - \frac{2(l_y n_x + l_x n_y) e_1}{3s_1 + s_2} - \frac{(l_y m_x + l_x m_y) e_2}{s_2} \right) \lambda_k \right]^t. \quad (2)
 \end{aligned}$$

We choose $\Delta=0.01$ for all our calculations. (The phase boundaries shown in Fig. 1 exhibit a weak dependence on Δt . However, provided Δt is chosen small enough, this dependence may be neglected.) The superscript t indicates that the values of the variables are taken at the t th discrete time step [27]. The control parameters are the dimensionless shear rate $\dot{\gamma}$ and λ_k . In place of the five coupled ODEs used in the conventional parametrization of the dynamics of \mathbf{Q} , we have six equations constrained by the normalization requirement, thereby conserving the number of degrees of freedom.

In our numerical analysis of the map, we start typically from random initial conditions, omitting sufficient transients ($\sim 10^5$ time steps) to ensure that the asymptotic attractor of the dynamics is reached. Our analysis includes inspection of the (i) power spectrum, (ii) phase portraits, (iii) bifurcation diagrams, and (iv) time series of the different relevant variables.

Figures 2 and 3 show the variety of states obtained in our numerical calculations. Each subfigure, labeled as Figs. 2(a)–2(c) and Figs. 3(a)–3(c), has the following structure: The first inset, labeled (i) for all figures, describes the time dependence of n_z , the z component of the director, and the angle ϕ made by the projection of the director on the x - y plane with the x axis. The second inset, labeled (ii) for all figures, plots the quantities measuring the amount of ordering along the director and subdirector against each other, providing the attractor of the system in the s_1 - s_2 plane for a generic initial condition. The main panel in each of the subfigures shows the power spectrum of s_1 , $\log_{10}[|A(f)|^2]$, against frequency f on a semilogarithmic plot.

The following states are easily identified: (I) An aligned state denoted as A in the phase diagram of Fig. 1, but omitted, for brevity, from the states shown in Fig. 2 and Fig. 3. In the aligned state, neither the frame orientation, nor s_1 and s_2 , vary in time. The director is aligned with the flow at a fixed angle; (II) a tumbling state, in which the director lies in the shear plane (the xy plane) and rotates about the vorticity direction (the z axis). Figure 2(a)(i) indicates that this state is a stable in-plane state, since the z component of the director is zero. Also, the angle made by the projection of the director

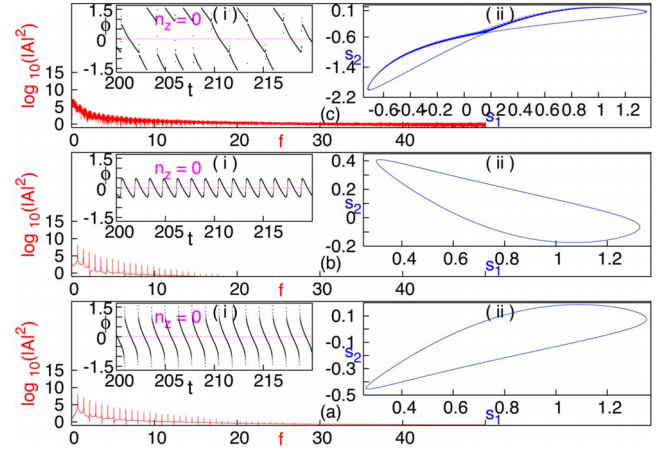


FIG. 2. (Color online) The sequence of three main panels shows the power spectrum associated with states in the regimes labeled (a) T and (b) W in the phase diagram of Fig. 1. The topmost panel (c) shows a mixed state (m) (not shown separately in Fig. 1), associated with the boundary between W and T. The inset labeled (i) in all of these panels shows typical plots of the time dependence of the z component of the director n_z and the angle ϕ made by the projection of the director on the x - y plane with the x axis. The insets labeled (ii) in all of these panels show the trajectory in the s_1 - s_2 plane.

on the x - y plane varies smoothly between $\pi/2$ and $\pi/2$. Figure 2(a)(ii) shows the periodic character of this state. This state is labeled as T in the phase diagram of Fig. 1; (III) a wagging state, in which the director lies in the shear plane, but oscillates between two values. Note that Fig. 2(b)(i) indicates that this state is a stable in-plane state. Also, the director oscillates back and forth in-plane as indicated in Fig. 2(b)(ii). Figure 2(b) shows that this state is a periodic state

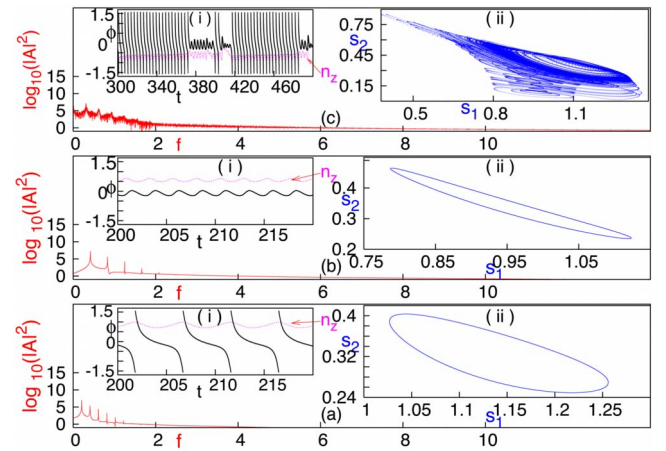


FIG. 3. (Color online) The sequence of three main panels shows the power spectrum associated with states in the regimes labeled (a) KT (kayak-tumbling), (b) KW (kayak-wagging), and (c) C (complex or chaotic) in the phase diagram of Fig. 1. The inset labeled (i) in all these panels shows typical plots of the time dependence of the z component of the director n_z and the angle ϕ made by the projection of the director on the x - y plane with the x axis. The insets labeled (ii) in all of these panels show the trajectory in the s_1 - s_2 plane.

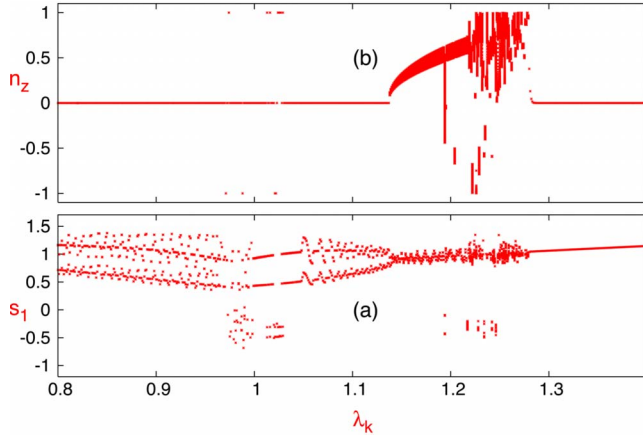


FIG. 4. (Color online) Bifurcation diagram obtained for a generic initial condition by varying λ_k at fixed $\dot{\gamma}=4.0$, showing (a) n_z and (b) a Poincaré section of s_1 (with s_2 fixed at the midpoint of the s_2 range) at each point in the bifurcation diagram.

with sharp δ -function peaks in the power spectrum. These states are denoted as W in the phase diagram in Fig. 1.

In addition to the states described above, we obtain (IV) a kayak-tumbling state, equivalent to the tumbling state, but in which the director is out of the shear plane. Thus, as shown in Fig. 3(a) $n_z \neq 0$ and the projection of the director on the xy plane rotates through a full cycle. Such states are temporally periodic, as shown in Fig. 3(a); the regular cycles evident in the map of s_1 vs s_2 [Fig. 3(a)(ii)] is a further indication of periodic behavior. These states are noted as KT in the phase diagram of Fig. 1; (V) a kayak-wagging state where, as in KT, the director is out of plane, but the projection of the director on the shear plane oscillates between two values. The properties of such states are illustrated in Fig. 3(b). Such states are again temporally periodic. The cyclic trajectory of the system in the s_1 - s_2 plane [Fig. 3(b)(ii)] further confirms such periodic behavior. These states are denoted by KW in the phase diagram of Fig. 1; (VI) a mixed state, typically found close to the boundaries between wagging and tumbling states, whose properties are illustrated in Fig. 2(c). In such states, the director exhibits both oscillation and complete rotations. Power spectra obtained at the boundaries of this phase, for example, near $\lambda_k=0.99$ and $\dot{\gamma}=4.0$, have a broad range of frequencies; and (VII) a complex state, in which the director lies out of the shear plane but both oscillates and rotates. The complex phase exhibits chaotic behavior, as can be seen in Fig. 3(c). Note that the δ function peaks in the power spectrum exhibited by the periodic states discussed earlier have broadened into a continuum of frequencies. The plot of s_1 vs s_2 displays no regular structure. These states are noted as C in the phase diagram in Fig. 1. In addition to these states, we also obtain a log-rolling state in which the director is perpendicular to the shear plane (not shown).

The range of dynamical states manifest in this problem is clearly evident in the bifurcation diagram of Fig. 4 which shows a cut in the phase diagram at fixed $\dot{\gamma}=4.0$, varying λ_k . Such a cut intersects KT, T, W, KW, C, and A states in the

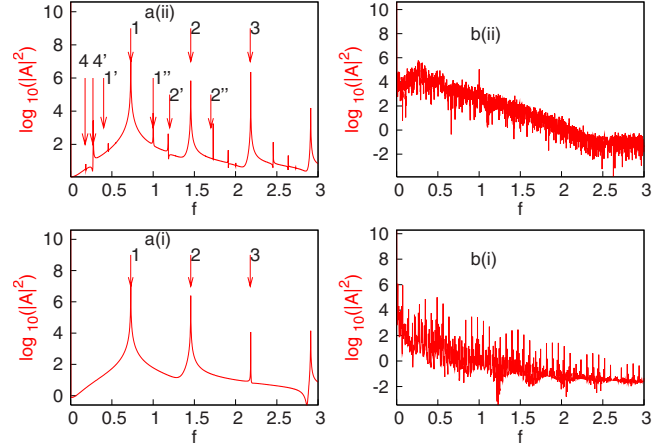


FIG. 5. (Color online) The two upper panels (a)(ii) and (b)(ii) show the power spectrum of s_1 against frequency f on a semilogarithmic plot for states corresponding to a representative point in the regimes labeled (a) T and (b) C (complex or chaotic) in the phase diagram of Fig. 1. We choose $\dot{\gamma}$ to vary periodically with frequency ω_a , and take $\dot{\gamma}_1=0.1$. The lower panel, labeled (a)(i) and (b)(i), in both cases shows the unperturbed power spectrum. The frequency peaks indicated in (a)(i), the system without periodic forcing, are indexed as follows: 1=0.729 (the fundamental frequency), 2 = 1.456 (2 times the fundamental frequency), and 3=2.174 (3 times the fundamental frequency). The fundamental frequency of the applied signal is shown as 4=0.184. The primed peaks indicated in (a)(ii) are combinations of the intrinsic frequency and the frequency of the applied signal and indexed as follows: 1' = 1 - 4', 2' = 2 - 4', 1'' = 1 + 4'. Note that the broad-band structure of the power spectrum in (b)(i) remains intact when the forcing is applied.

phase diagram. For specificity we show the quantities n_z and the Poincaré section of s_1 . It is clearly evident from Fig. 4 that $n_z=0$ for the T, W, and A states, while the KT, KW, and C states are out-of-plane states with $n_z \neq 0$. Further, the s_1 section, shows a fixed point for the aligned state, regular cycles for the KT, T, W, and KW states, and irregular (chaotic) behavior for the C state.

Finally, we investigate the behavior of this dynamical system to a class of periodic perturbations constructed by taking $\dot{\gamma} = \dot{\gamma}_0 + \dot{\gamma}_1 \sin(\omega_a t)$, with t taken in discrete time and ω_a representing the angular frequency of the applied forcing. This corresponds to the experimental situation in which the steady shear is modulated by a small ($\dot{\gamma}_1 \ll 1$) amplitude periodic perturbation. If $\dot{\gamma}_0$ were strictly zero, this would be the case of purely oscillatory shear. We choose ω_a to be small, so that steady state is easily achieved. We have also investigated the effects of periodic variation of λ_k , finding behavior similar to that described below.

Our results are summarized in Fig. 5 which show the power spectrum of s_1 , $\log_{10}(|A(f)|^2)$ against frequency f on a semilogarithmic plot. Data for the states labeled (a) T and (b) C in the phase diagram of Fig. 1 are shown. For comparison, we show the unperturbed power spectrum in the lower panel of each figure. Note that the introduction of the time modulation adds an additional periodic component to the signal in the case of the periodic states, such as the T state. The power spectrum shows several harmonics of the intrinsic and driv-

ing frequencies as well as linear combinations of these frequencies, consistent with the inherent nonlinearity of this system. The peaks in the power spectrum are indexed as shown in the figure. For the state labeled (C) (complex or chaotic), the power spectrum shows broad-band structure as before, indicating that the periodic driving does not serve to stabilize order. These statements remain roughly independent of the amplitude of the periodic perturbation, provided it is not large enough that nearby states in the phase diagram are accessed. The generic features described above continue to hold in the other regions of the phase diagram.

Aradian and Cates have recently studied a minimal model for rheochaos in shear-thickening fluids, using equations which describe a shear-banding system coupled to a retarded stress response [29]. These authors connect their model system to a modified Fitzhugh-Nagumo model, a dynamical system with a variety of interesting and complex phases. Fielding and Olmsted studied instabilities in shear-thinning fluids, where the instability originates in the multibranch character of the constitutive relation [30]. Chakrabarty *et al.* reported a study of the PDEs describing the dynamics of \mathbf{Q} , characterizing spatiotemporal routes to chaotic behavior in sheared nematics [22]. All of these studies allow for spatial variation—although restricted so far to the one-dimensional case—whereas our local map describes the spatially uniform

situation. However, the dynamical system we study is obtained directly from the underlying dynamics, in contrast to the approaches of Refs. [29,30]. Whether coupling maps of the sort we construct permits a complete description of the spatiotemporal structure obtained in Ref. [22] remains to be seen.

In conclusion, we have proposed a local map describing the variety of dynamical states obtained in a model for sheared nematics. Our phase diagram, Fig. 1, contains all nontrivial dynamical states obtained in previous work. It also closely resembles, even quantitatively, phase diagrams obtained in previous work which used ordinary differential equations formulated in continuous time. We have also studied the behavior of the map under parametric oscillations of the shear rate, a physical situation not addressed earlier. Our work thus supplies a crucial ingredient in the construction of coupled map lattice approaches to the spatiotemporal aspects of rheological chaos, a problem currently at the boundaries of our understanding of the dynamics of complex fluids.

The authors thank Rajaram Nityananda, A. K. Sood, Sriram Ramaswamy, Chandan Dasgupta, and Ronojoy Adhikari for discussions. This work was partially supported by the DST (India) (G.I.M.).

-
- [1] O. Diat, D. Roux, and F. Nallet, *J. Phys. II* **3**, 1427 (1993).
 [2] V. Schmitt *et al.*, *Langmuir* **10**, 955 (1994).
 [3] J.-F. Berret *et al.*, *J. Phys.: Condens. Matter* **8**, 9513 (1996).
 [4] E. Eiser, F. Molino, G. Porte, and O. Diat, *Phys. Rev. E* **61**, 6759 (2000).
 [5] J.-B. Salmon, A. Colin, and D. Roux, *Phys. Rev. E* **66**, 031505 (2002).
 [6] R. Bandyopadhyay, G. Basappa, and A. K. Sood, *Phys. Rev. Lett.* **84**, 2022 (2000); A. K. Sood, R. Bandyopadhyay, and G. Basappa, *Pramana* **53**, 223 (1999); R. Bandyopadhyay, G. Basappa, and A. K. Sood, *Europhys. Lett.* **56**, 447 (2001).
 [7] Rajesh Ganapathy and A. K. Sood, *Langmuir* **22**, 11016 (2006); *Phys. Rev. Lett.* **96**, 108301 (2006).
 [8] P. E. Cladis and W. van Saarloos, in *Solitons in Liquid Crystals*, edited by L. Lam and J. Prost (Springer, New York, 1992), pp. 136–137.
 [9] M. E. Cates and S. M. Fielding, *Adv. Phys.* **55**, 799 (2006).
 [10] P. D. Olmsted and C.-Y. D. Lu, *Faraday Discuss.* **112**, 183 (1999).
 [11] S. Hess, *Z. Naturforsch. A* **31A**, 1034 (1976).
 [12] M. Doi, *J. Polym. Sci., Polym. Phys. Ed.* **19**, 229 (1981).
 [13] M. Doi and S. F. Edwards, *The Theory of Polymer Dynamics* (Oxford University Press, London, 1986).
 [14] S. Hess and I. Pardowitz, *Z. Naturforsch. A* **36A**, 554 (1981).
 [15] C. Pereira Borgmeyer and S. Hess, *J. Non-Equilib. Thermodyn.* **20**, 359 (1995).
 [16] N. Kuzuu and M. Doi, *J. Phys. Soc. Jpn.* **52**, 3486 (1983).
 [17] P. D. Olmsted and P. M. Goldbart, *Phys. Rev. A* **41**, 4578 (1990); **46**, 4966 (1992).
 [18] H. Stark and T. C. Lubensky, *Phys. Rev. E* **67**, 061709 (2003), and references therein.
 [19] M. Grosso, R. Keunings, S. Crescitelli, and P. L. Maffettone, *Phys. Rev. Lett.* **86**, 3184 (2001).
 [20] G. Rienäcker, M. Kröger, and S. Hess, *Phys. Rev. E* **66**, 040702 (2002).
 [21] G. Rienäcker, M. Kröger, and S. Hess, *Physica A* **315**, 537 (2002).
 [22] B. Chakrabarti, M. Das, C. Dasgupta, S. Ramaswamy, and A. K. Sood, *Phys. Rev. Lett.* **92**, 055501 (2004).
 [23] M. Das, B. Chakrabarti, C. Dasgupta, S. Ramaswamy, and A. K. Sood, *Phys. Rev. E* **71**, 021707 (2005).
 [24] *Theory and Applications of Coupled Map Lattices*, edited by K. Kaneko (Wiley, New York, 1993).
 [25] As is common in high-dimensional complex systems, there is a possibility of coexistence of different dynamical states; our phase diagram shows the dominant attractor of the dynamics.
 [26] S. L. Altmann, *Rotations, Quaternions, and Double Groups* (Dover, New York, 1986).
 [27] These equations are apparently singular in the three limits $s_2 \rightarrow 0$, $3s_1 + s_2 \rightarrow 0$, and $3s_1 - s_2 \rightarrow 0$, when denominators containing these quantities approach zero. This happens at isolated points in the dynamical evolution of the map, when the system is rendered effectively uniaxial, as a consequence of eigenvalues along two orthogonal axes becoming degenerate. We deal with this in two ways. First, we can set these terms the denominator to a small constant whenever they reach a preset value close to zero, so that these terms never actually cross zero. Alternatively, we may use the freedom to choose the degenerate eigenvectors in such a way as to cancel the term

which vanishes in the denominator. In practice, both schemes give equivalent results. We also note that the system is always effectively biaxial due to the shear.

[28] In contrast to Ref. [21], the phase boundary between T and KT phases is somewhat diffuse, admitting the possibility of coexistence states sufficiently close to the boundary. Such states

become increasingly rare at large values of $\dot{\gamma}$ and are suppressed as Δ is made smaller. Also, the chaotic region has a marginally different shape in our calculations.

[29] A. Aradian and M. E. Cates, Phys. Rev. E **73**, 041508 (2006).

[30] S. M. Fielding and P. D. Olmsted, Phys. Rev. Lett. **92**, 084502 (2004).